Structural and Biochemical Characterization of the Nucleosome Containing Variant H3.3 and H2A.Z

Harry Jung , Vladyslava Sokolova , Gahyun Lee , Victoria Stevens , Dongyan Tan *

Posted Date: 29 March 2024

doi: 10.20944/preprints202403.1829.v1

Keywords: histone variants; H2A.Z; H3.3; nucleosome; chromatin

Article

Structural and Biochemical Characterization of the Nucleosome Containing Variant H3.3 and H2A.Z

Harry Jung [1,2†], Vladyslava Sokolova [1†], Gahyun Lee [1], Victoria Steven [1,3] and Dongyan Tan [1*]

[1] Department of Pharmacological Sciences, Stony Brook University; Stony Brook, New York, 11794.
[2] Department of Pharmacology, Yale University, New Haven, Connecticut, 06520 (current affiliation)
[3] Chembio Diagnostics Systems Inc, Medford, NY 11763 (current affiliation)
* Correspondence: To whom correspondence should be addressed. Tel: 1-631-638-1286; Email: dongyan.tan@stonybrook.edu.
† These authors contributed equally to this work.

Abstract: Variant H3.3, along with H2A.Z, is notably enriched at promoter regions and is commonly associated with transcriptional activation. However, the specific molecular mechanisms through which H3.3 influences chromatin dynamics at transcription start sites, and its role in gene regulation, remain elusive. Using a combination of biochemistry and cryo-electron microscopy (cryo-EM), we show that the inclusion of H3.3 alone does not induce discernible changes in nucleosome DNA dynamics. Conversely, the presence of both H3.3 and H2A.Z enhances DNA flexibility similarly to H2A.Z alone. Interestingly, our findings suggest that the presence of H3.3 in the H2A.Z nucleosome provides slightly increased protection to DNA near the superhelical location (SHL) -5.5/5.5. These results imply that while H2A.Z at active promoters promotes the formation of more accessible nucleosomes with increased DNA accessibility to facilitate transcription, the simultaneous presence of H3.3 offers an additional mechanism to fine-tune nucleosome accessibility and the chromatin environment.

Keywords: histone variant; H3.3; H2A.Z; nucleosome; chromatin

1. Introduction

The regulation of gene expression in eukaryotes are achieved through alteration in chromatin structure and functions at the level of nucleosomes and higher-order structures. The epigenetic mechanisms exist to regulate this process include histone post-translational modifications (PTMs), ATP-dependent chromatin remodeling, and replacement of canonical histones with nonallelic histone variants. The deposition and removal of histone variants is a key epigenetic mechanism that have functional role in multiple nuclear processes. Unlike their canonical counterparts, which are synthesized and incorporated during S-phase [1], histone variants are expressed throughout the cell cycle [2]. The process to deposit and remove histone variants require the action of histone chaperones and/or ATP-dependent chromatin remodelers. Given their important and specialized functions in genome regulation, it is therefore not surprising that variant dysregulation are implicated in a variety of diseases such as tumorigenesis and developmental defects [3].

Several histone variants are known to involve in transcriptional control. Among them is variant H2A.Z, an essential protein for the survival of several organisms [4–7]. Variant H2A.Z shares only ~60% sequence identity with its canonical counterpart H2A, yet it is highly conserved across species (**Figure 1A**). H2A.Z has been linked to both transcription activation and repression. On one hand, H2A.Z is predominantly located at the distal end of inducible promoter (the so-called +1 nucleosome adjacent to the nucleosome free region at the promoter). This localization is crucial to poise the gene for rapid activation [8–12]. Upon transcription activation, H2A.Z is removed and replaced by the canonical histone H2A [13–15]. Nevertheless, substantial amount of H2A.Z is also found at heterochromatin regions such as centromere and pericentromeric heterochromatin [16–20], as well as in the gene body of repressed genes [21,22]. Recent studies, including ours, revealed that the incorporation of H2A.Z increases the accessibility of entry/exit DNAs on nucleosomes [23,24].

 doi:10.20944/preprints202403.1829.v1

Furthermore, we demonstrate that H2A.Z enables nucleosome arrays to fold into a more regular and compact chromatin fiber in vivo [23].

A second histone variant, H3.3, is primarily found in active transcribing genes, promoters, and gene regulatory elements. It is generally considered as an active mark for transcription [25–27]. Contrary to H2A.Z, H3.3 is different from the canonical H3 histone only in four or five amino acids (**Figure 1B**). An early study found that H3.3 nucleosomes are much more susceptible to salt-dependent disruption than canonical nucleosomes [28]. Nevertheless, later studies showed conflicting results, indicating that H3.3 alone have a negligible effect on nucleosomes structure [29] and stability in vivo [30]. Therefore, it remains unclear how H3.3-specific features contribute to distinct properties in H3.3 nucleosomes.

Nucleosomes containing both H2A.Z and H3.3 variants also exist *in vivo*, primarily located downstream of the nucleosome-free regions of active promoters [26,28]. The physical properties and stability of these double-variant nucleosomes remain controversial. Initially, double-variant nucleosomes isolated from vertebrates were shown to be unstable and sensitive to salt-dependent disruption, with a tendency to lose H2A.Z/H2B dimers [28]. However, another study found only subtle changes in the stability of these double-variant nucleosomes in vitro [31]. Beyond the nucleosome level, variant H3.3 was shown to inhibit H2A.Z-mediated chromatin higher-order structure formation [30]. This raises questions about how variant H3.3 interfaces with H2A.Z to modulate chromatin structure and function at different chromatin regions.

Several recent cryo-EM studies shed light on variant-specific changes in nucleosome and chromatin. Despite the different variants involved, a common theme emerges: histone variants exert their influence on chromatin by modulating DNA near the entry/exit sites [32]. To further understand H3.3-mediated chromatin changes and transcriptional regulation, we compared nucleosomes containing canonical histones, variants H2A.Z, and H3.3 (in isolation and in combination with H2A.Z) using DNA accessibility assays to assess variant-dependent DNA dynamics. Our biochemical data show that H3.3 alone does not alter linker DNA accessibility on nucleosomes. However, the presence of variant H2A.Z, either alone or with H3.3, substantially increases entry/exit DNA flexibility within the nucleosome. Consistent with this biochemical data, our cryo-EM structure of the H2A.Z-H3.3 double-variant nucleosome reveals a remarkably similar overall structure compared to the H2A.Z nucleosome, displaying asymmetric DNA wrapped around the histone octamer. Furthermore, our study revealed that the INO80-dependent chromatin remodeler exhibits similar DNA translocation activity on double-variant nucleosomes compared to H2A.Z nucleosomes. Together, these findings suggest that variant H3.3 alone does not alter the entry/exit DNA accessibility on nucleosomes. The concurrent presence of H3.3 with H2A.Z, on the other hand, resembles the effect of H2A.Z on nucleosome stability and DNA dynamics. Intriguingly, the double-variant nucleosome displays a small but significant decrease in DNA accessibility near the superhelical location (SHL) -5.5/5.5 compared to H2A.Z nucleosome in our assay. We propose that the presence of H2A.Z leads to the formation of more accessible nucleosomes with increased DNA ends to facilitate transcription. The concurrent presence of H3.3 offers an additional mechanism to fine-tune nucleosome DNA accessibility and thus chromatin environment at promoters and gene regulatory elements.

 doi:10.20944/preprints202403.1829.v1

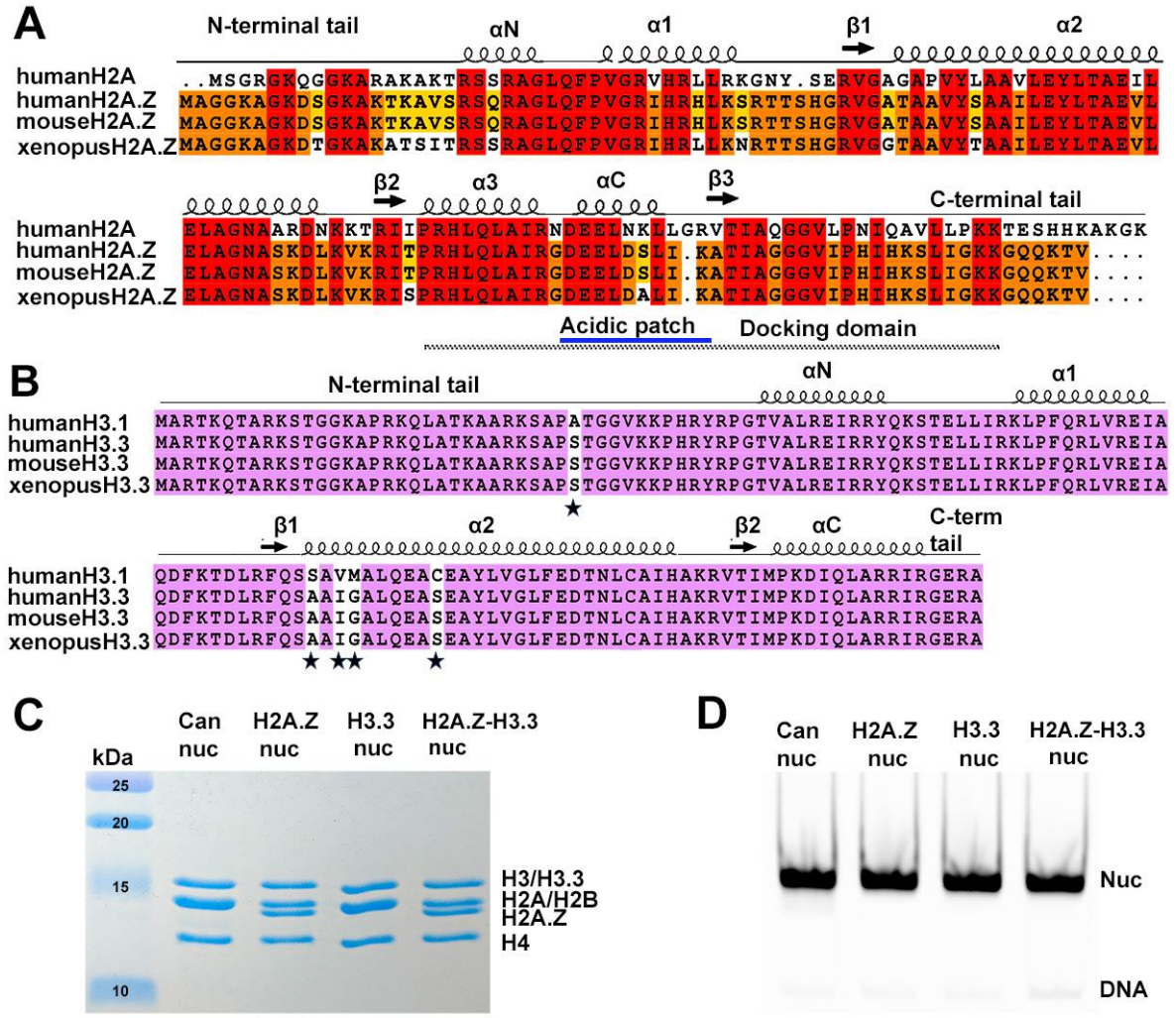

Figure 1. Sequence conservation of histone variants and nucleosome preparation. (**A**) Sequence alignment of variant H2A.Z and canonical H2A, showing identical sequence between mouse and human H2A.Z. Conserved amino acids are in red. Structural elements are indicated above alignment. Docking domain indicated as dotted line under the alignment. (**B**) Sequence alignment of canonical H3.1 and variant H3.3, showing identical sequence between mouse and human H3.3. Conserved amino acids are in purple. The five amino acid substitutions are marked by asterisk. (**C**) 15% Coomassie-stained SDS-PAGE gel shows purified histone octamers used in the current study. (**D**) 3% Native-PAGE shows in vitro reconstituted nucleosomes used in the current study.

2. Material and Methods

2.1. Protein Production

Histones H2A, H2B and H4, and H3 from *Xenopus laevis* were expressed in BL21 (DE3) pLysS *E. coli* cells and purified according to the established procedures [33]. The mouse H3.3 gene was re-cloned into pET-LIC expression vector from mCerulean-H3.3-N-14, which was a generous gift from Michael Davidson (Addgene plasmid # 55377; http://n2t.net/addgene:55377; RRID: Addgene_55377). The mouse H2A.Z.1 gene in pIND-EGFP was a generous gift from Danny Rangasamy (Addgene plasmid # 15770; http://n2t.net/addgene:15770; RRID:Addgene_15770). It was re-cloned into pET-LIC expression vector. Histones H3.3 and H2A.Z were expressed in BL21 (DE3) *E. coli* cells and purified following the same protocol.

All histone octamers used in this study were produced in vitro through refolding as previously described [33]. Briefly, al histones were mixed in equal molar concentrations and incubated for 2 hours in unfolding buffer (7 M guanidine HCl, 20 mM Tris, pH 7.5, and 10 mM DTT) followed by

 doi:10.20944/preprints202403.1829.v1

dialysis against at least three changes of refolding buffer (10 mM Tris, pH 7.5, 1 mM EDTA, 2 M NaCl and 1 mM DTT) at 4°C. The octamers were concentrated and purified by gel filtration using a Superdex200 increase 10/300 GL column.

2.2. DNAs

A plasmid containing twelve tandem repeats of 167-bp 601 Widom sequence was used. 167-bp nucleosomal DNA was liberated by EcoRV restriction enzyme digestion. Subsequently, DNA fragments were further purified by anion exchange chromatography using an HQ Poros column (Applied Biosciences). The sequence used for reconstituting nucleosomes is listed below with the 601 sequence underlined:
ATCCCGCCCTGGAGAATCCCGGTGCCGAGGCCGCTCAATTGGTCGTAGACAGCTCTAGCACCGCTTAAACGCACGTACGCGCTGTCCCCCGCGTTTTAACCGCCAAGGGGATTACTCCCTAGTCTCCAGGCACGTGTCAGATATATACATCCTGTGCATGACTAGAT

The plasmid with twelve tandem repeats of 208-bp 601 Widom sequence was a generous gift from Dr. Ed Luk. Restriction enzyme ScaI was used to liberate single repeat of 208-bp segment. DNA fragments were further purified by anion exchange chromatography using HQ Poros column (Applied Biosciences). The sequence is as follows with the 601 sequence underlined:

ACTTATGTGATGGACCCTATACGCGGCCGCCCTGGAGAATCCCGGTGCCGAGGCCGCTCAATTGGTCGTAGACAGCTCTAGCACCGCTTAAACGCACGTACGCGCTGTCCCCCGCGTTTTAACCGCCAAGGGGATTACTCCCTAGTCTCCAGGCACGTGTCAGATATATACATCCTGTGCATGTATTGAACAGCGACCTTGCCGGAGT

End-positioned 0N80 (80 base pairs of extra-nucleosomal DNA at one entry/exit site) Widom DNA was amplified by PCR using primers (0N80-F 5'-CTGGAGAATCCCGGTGCCGAG-3' and 0N80-R 5'-TCGGTACCCGGGGATCCTCTA-3') and the plasmid pGEM-3z/601, a generous gift from Jonathan Widom (Addgene plasmid #26656). The sequence is as follows with the 601 Widom sequence underlined:

CTGGAGAATCCCGGTGCCGAGGCCGCTCAATTGGTCGTAGCAAGCTCTAGCACCGCTTAAACGCACGTACGCGCTGTCCCCCGCGTTTTAACCGCCAAGGGGATTACTCCCTAGTCTCCAGGCACGTGTCAGATATATACATCCTGTGCATGTATTGAACAGCGACCTTGCCGGTGCCAGTCGGATAGTGTTCCGAGCTCCCACTCTAGAGGATCCCCGGGTACCGA

2.3. Nucleosome Reconstitution

Nucleosomes were reconstituted by mixing the octamer with the 601 Widom DNA in equal molar ratio in high-salt buffer [10 mM Tris, pH 8.0, 2 mM EDTA, 2 M NaCl and 2 mM 2-Mercaptoethanol (βME)] followed by overnight dialysis into low salt buffer (10 mM Tris, pH 8.0, 2 mM EDTA, 5 mM NaCl and 2 mM βME) as described [33]. For the HinfI endonuclease digestion assay, 208-bp 601 DNA was used for nucleosome production. To produce nucleosomes for the Cryo-EM experiments and the MNase digestion assay, 167-bp 601 DNA was used. To produce nucleosomes for the ATP-dependent nucleosome-sliding assay, the end-position 0N80 DNA was used.

2.4. HinfI Endonuclease Accessibility Assay

250 nM of 208 bp nucleosome was mixed with 45 U of endonuclease enzyme HinfI in Cutsmart buffer (NEB) (20 mM Tris-Ac, pH7.9, 50 mM KAc, 10 mM MgAc, 100 µg/ml BSA) in total volume of 45 µl and incubated at 37°C. Samples were collected every 15 min (5 µl) and the reaction was quenched with 8 µl of stop buffer (10 mM Tris–HCl, pH 8.0, 0.6% SDS, 40 mM EDTA, 0.1mg/ml Proteinase K) immediately. Samples were then incubated at 50°C for 1 hour for deproteination, followed by separation on 8% Native-PAGE gels. The gels were stained with SYBR GOLD, imaged on a Typhoon imager (Cytiva). Quantitative analysis was done using ImageJ software version 1.53e. The level of significant difference was determined using a Two-way ANOVA test with $P \leq 0.05$ considered significant. Graphical representation and Two-way ANOVA tests were conducted using Prism 5 software.

 doi:10.20944/preprints202403.1829.v1

2.5. MNase Accessibility Assay

In the MNase accessibility assay, 425 nM of 167-bp nucleosomes in a 65 µl volume were subjected to digestion with 0.75 U of MNase (Roche) in buffer (10 mM Tris pH 7.4, 50 mM NaCl, 2 mM CaCl2) in a total volume of 65 µl at 37°C. Samples (4.5 µl) were collected every 3 minutes, quenched with 10 µl of stop buffer (10 mM Tris pH 7.5, 40 mM EDTA, 0.6% SDS, 0.1 mg/ml proteinase K), and then incubated at 50°C for 1 hour. The samples were resolved on a Native-PAGE gel (19:1 Acrylamide/Bis, 2.5% stacking gel with 8% resolving gel) at 4°C (100 V, 180 min, 1x TBE) followed by staining with SYBR-GOLD (GoldBio). The gels were imaged on a Typhoon imager (Cytiva). Quantitative analysis of the gels was performed using ImageJ software. Intensities for DNA fragments were estimated cumulatively from bands of similar size. The percentage change of DNA fragments over time was plotted. The two-way ANOVA test was employed to determine the statistical significance between datasets using the criterion $p \leq 0.05$. Two-way ANOVA tests and graphical representations were conducted using Prism 5 software.

2.6. Nucleosome Sliding Assay

200 nM of end-positioned nucleosomes (0N80) were mixed with INO80-C complexes (50 nM) in sliding buffer (25 mM HEPES pH 8.0, 50 mM NaCl, 5% glycerol, 1 mM TCEP, and 2 mM MgCl2) in a final volume of 10 µl. The reactions were incubated at 37°C for 10 minutes. Sliding was initiated by adding 1 mM ATP at 24°C, and the reaction was quenched by adding 5 mM EDTA and 0.2 mg/ml lambda DNA (NEB). Reactions at different time points were collected and resolved on 6% Native-PAGE gels at 4°C (100 V, 120 min, 1x TBE). Gels were stained with SYBR-GOLD (GoldBio) before imaging on a Typhoon imager (Cytiva).

2.7. Vitrification

The reconstituted double-variant nucleosomes were concentrated to a final concentration of 6 µM. The samples were cross-linked with 0.1% glutaraldehyde for 15 minutes on ice, and the reaction was quenched by adding Tris (pH 8.0) to a final concentration of 50 mM. Vitrification was performed using a Vitrobot Mark IV (FEI Company) at 8°C and 100% humidity. Aliquots of 3.5 µl of the nucleosome sample were applied to glow-discharged QUANTIFOIL UltraAuFoil grids with 100 Holey Gold support (R1.2/1.3 – 300 mesh), blotted for 4 to 5 seconds, and plunged into liquid ethane cooled by liquid nitrogen. Grids were stored in liquid nitrogen until they were imaged.

2.8. Cryo-EM Data Collection

Grid screening was conducted in the Talos Arctica microscope at the cryo-EM facility at Stony Brook University. Two optimal grids were selected for data collection, which took place at the UVA Molecular Electron Microscopy Core with the Titan Krios Microscope operating at 300 kV with a Bioquantum energy filter set to zero loss frequency (10 eV). Movies were recorded using a K3 direct electron detector (Gatan Company) in counting mode with EPU software at 81,000X magnification, resulting in a pixel size of 1.08 Å at the specimen level. Defocus values ranged from 1.0 to 2.25 µm. Each movie was dose-fractionated into 40 frames with a dose rate of approximately 1.25 e/pixel/sec. The total exposure time was 2.5 seconds, corresponding to a total dose of 50 e/Å^2 per micrograph (Supplementary Data Table 1). A total of 5140 movies were collected with the two grids.

2.9. Image Processing

From the initial dataset, 2673 movies were selected for further data processing after a thorough inspection to remove any suboptimal movies. Movie frames were aligned and summed using MotionCor2 software with patch motion correction [34]. The CTF parameters were estimated using CTFFIND4 [35]. Reference-based auto particle picking was carried out in RELION [36], resulting in a dataset of ~1.2 million particles. Poor-quality particles were removed through 2D classification. Particles from the good class averages were pooled and subjected to 3D classification. The best class, containing 205,792 particles, was re-extracted without binning and re-centered, then subjected to

 doi:10.20944/preprints202403.1829.v1

consensus 3D refinement. Postprocessing, CTF refinement, and Bayesian Polishing were performed using this consensus refined map. No symmetry was applied during refinement. These procedures yielded a final map with an average resolution of 3.0 Å.

2.10. Model Building and Refinement

The histone core from H2A.Z nucleosome containing H3.3 (PDB: 5B33) and the 601 DNA sequence from the canonical nucleosome (PDB: 6FQ5) were combined to generate the initial model used for model refinement. This initial model was manually fitted into the density map using UCSF ChimeraX [37], followed by manual rebuilding using Coot [38]. The model was further refined using Phenix.real_space_refine [39]. The model geometry was checked and further idealized according to standard geometry restrains through geometry minimization in Phenix. Statistics are presented in Supplementary Data Table 1. UCSF ChimeraX was used to visualized the density map and models, as well as preparing figures for publication.

2.11. Quantification and Statistical Analysis

For the experiments depicted in Figures 2 and S1, the average values of three independent experiments were presented alongside their respective standard deviations (SD). In both instances, consistent and reproducible results were achieved.

Preprints.org (www.preprints.org) | NOT PEER-REVIEWED | Posted: 29 March 2024 doi:10.20944/preprints202403.1829.v1

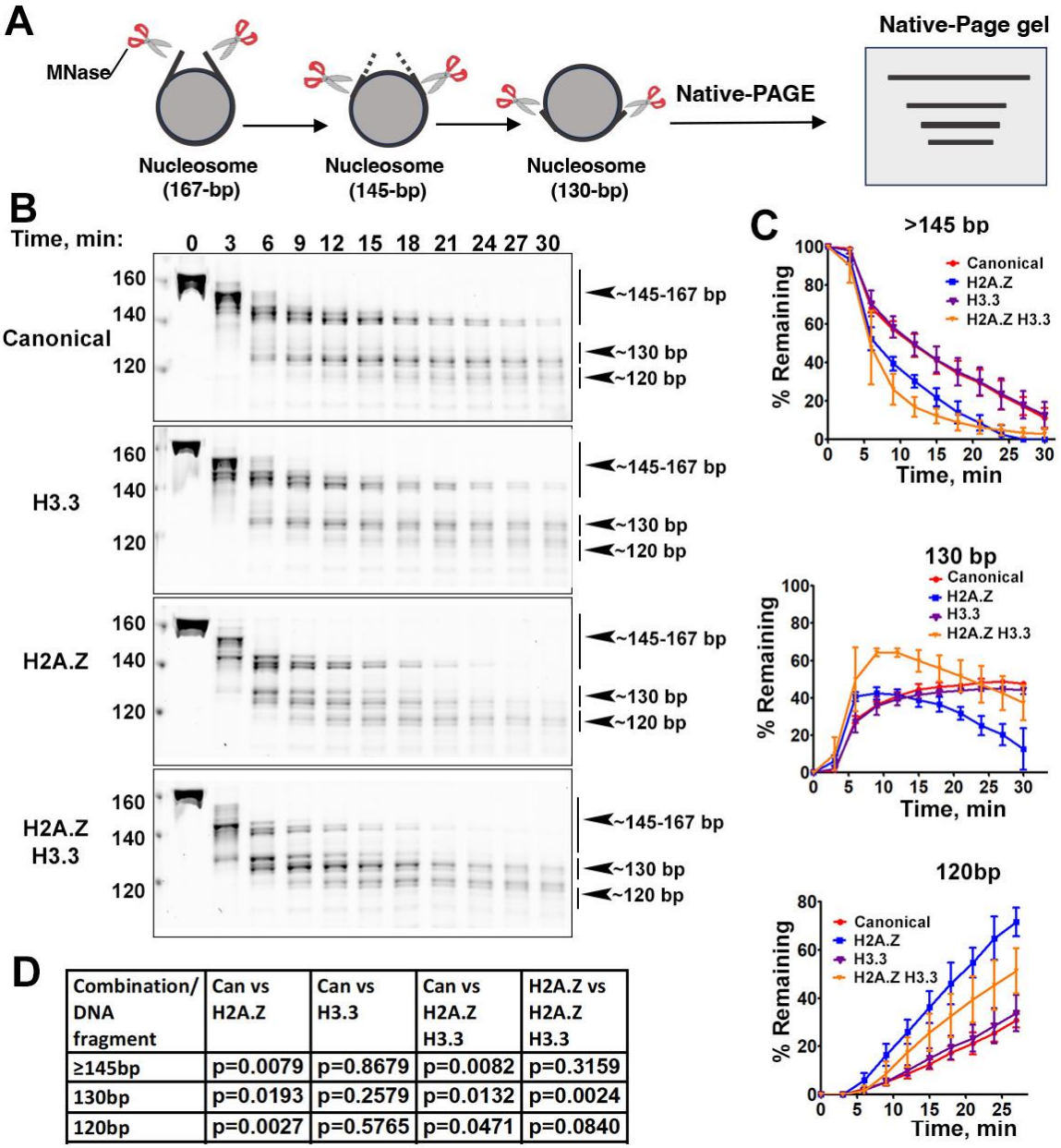

D

Combination/ DNA fragment	Can vs H2A.Z	Can vs H3.3	Can vs H2A.Z H3.3	H2A.Z vs H2A.Z H3.3
≥145bp	p=0.0079	p=0.8679	p=0.0082	p=0.3159
130bp	p=0.0193	p=0.2579	p=0.0132	p=0.0024
120bp	p=0.0027	p=0.5765	p=0.0471	p=0.0840

Figure 2. The effects of histone variants on nucleosome DNA accessibility assessed by MNase assay. (**A**) Schematic of the MNase digesion of nucleosomes. (**B**) Representative acrylamide gels of the MNase digestion of canonical, H3.3, H2A.Z and H2A.Z-H3.3 double-variant nucleosomes, respectively. The digestion products of different sizes (145-167, 130, 120) are labeled. (**C**) Quantification of the digestion DNA products shown in (B), representing the fraction of cleaved nucleosome DNA as a function of time. Data are mean ± SD, n = 3. (**D**) P values of the abovementioned quantification analysis, estimated by two-way Anova.

3. Results

3.1. The Incorporation of H2A.Z-H3.3 Double-Variants Enhances the Terminal DNA Accessibility on Nucleosomes

To reconstitute nucleosomes for structural and biochemical analysis, we used a DNA fragment containing the Widom 601 nucleosome-positioning sequence [40]. Mono-nucleosomes were reconstituted following an standard protocol [33] using recombinant proteins containing either canonical *Xenopus* histones, mouse histone variant H2A.Z.1, or human histone variant H3.3 (**Figure 1C,D**).

 doi:10.20944/preprints202403.1829.v1

Previous research has shown that incorporating H2A.Z increases the flexibility and accessibility of terminal DNAs compared to canonical nucleosomes, supported by both restriction enzyme-based assays and cryo-EM studies [23]. While it has been observed that H3.3 nucleosomes are more unstable and susceptible to salt disruption in vitro [28], their specific impact on entry/exit DNA dynamics remains unclear. To address this, we employed a Micrococcal nuclease (MNase)-based DNA accessibility assay to determine the influence of variant H3.3 and its combined effect with H2A.Z on nucleosome DNA accessibility. MNase, a sequence-independent endonuclease, preferentially digests accessible DNA ends on nucleosomes (**Figure 2A**). The results revealed three dominant DNA fragments (145, 130, and 120-bp) throughout digestion (**Figure 2B**). We analyzed and quantified the patterns of these fragments across various nucleosome substrates over time to assess the level of compaction or relative DNA accessibility on nucleosomes.

Our findings show that nucleosomes containing the H3.3 variant exhibit nearly identical DNA protection as canonical nucleosomes (**Figure 2C**), indicating that H3.3 alone does not induce detectable structural changes on the entry/exit DNA. In contrast, cleavage of terminal DNAs on H2A.Z nucleosomes, regardless of H3.3 variant presence, occurred significantly faster than in canonical nucleosomes, as evidenced by the rapid disappearance of the 145-bp fragment (top graph in **Figure 2C**)**.** This aligns with the notion that H2A.Z incorporation enhances DNA breathing at the entry/exit sites [23,24]. Intriguingly, digestion of the 130-bp fragment in the double-variant nucleosome slows down even though it continues to be degraded into smaller products in the H2A.Z nucleosome (middle graph in **Figure 2C**). This difference between the double-variant nucleosome and H2A.Z nucleosome is small but statistically significant (**Figure 2D**). Since the 130-bp fragment corresponds to cleavage near SHL -5.5/5.5, this observation suggests the existence of H3.3-dependent DNA protection near SHL -5.5/5.5 in the double-variant nucleosomes.

To corroborate the MNase results, we performed an additional assay employing the restriction enzyme HinfI, which targets a cleavage site proximal to SHL-6.5/6.5. The results show that HinfI digestion progresses notably faster for nucleosomes containing H2A.Z compared to canonical or H3.3-nucleosomes (**Figure S1**). Furthermore, it shows no significant difference in HinfI site accessibility between H2A.Z nucleosomes and H2A.Z-H3.3 double-variant nucleosomes. The outcome of this assay is consistent with the digestion pattern observed in the MNase assay concerning the 145-bp fragment (**Figure 2B,C**), Hence, our findings from the HinfI digestion assay reinforce those obtained from the MNase assay.

3.2. Cryo-EM Structure of the H2A.Z-H3.3 Double-Variant Nucleosome

We next performed single-particle cryo-EM on the H2A.Z-H3.3 double-variant nucleosome. 3D classification of the dataset shows all classes with asymmetric DNA ends (**Figure S2C**). The final density map at 3 Å resolution was calculated from the best class without imposing symmetry (**Figures 3A and S2**). Using this density map, we generated an atomic model of the double-variant nucleosome. The model closely resembles our previous H2A.Z nucleosome structure [23], featuring asymmetrically DNA wrapped around the histone core. The double-variant nucleosome model shows 128-bp of DNA, slightly shorter than the 136-bp DNA resolved in our previous H2A.Z nucleosome structure [23] (**Figure 4C**). The asymmetric wrapping of DNA is likely attributed to the asymmetry of the Widom 601 nucleosome-positioning sequence, as observed in other variant nucleosomes derived using the same synthetic DNA [32]. Previous studies indicates that variant H2A.Z accentuates this asymmetry compared to the canonical nucleosome[23].

 doi:10.20944/preprints202403.1829.v1

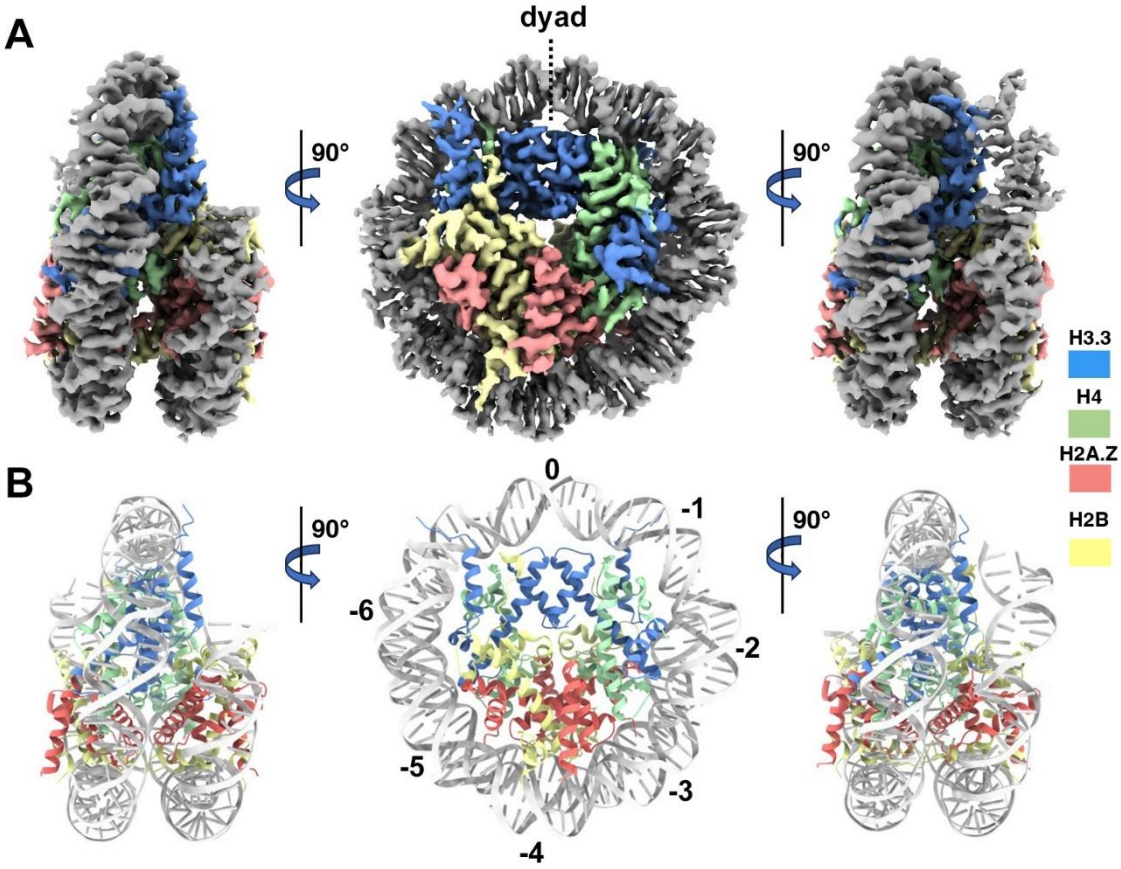

Figure 3. Cryo-EM structure of H2A.Z-H3.3 double-variant nucleosome. (**A**) Surface representation of the cryo-EM density map of the double-variant nucleosome shown in three different views. Densities of the DNA and different histones are color-coded according to the label shown on the right. (**B**) Atomic model of the double-variant nucleosome displayed in three different views corresponding to those in A. The color-codes for different molecules correspond to those in A. The superhelical locations are labeled with numbers for reference.

One of the five H3.3-specific residues is located at the N-terminal tail of the protein, remaining disordered and thus unresolved in our structure (**Figure 4A**). The other four amino acid substitution in variant H3.3 (A87, I89, G90, and S96) are part of the $\alpha 2$ helix, which adopts the same configuration as in the canonical histone H3.1 from our previous H2A.Z nucleosome model (**Figure 4B**). These amino acids, like their counterparts in histone H3.1 (S87, V89, M90, C96), are part of the hydrophobic residue group. This suggests that the amino acid substitutions in variant H3.3 are unlikely to alter the protein structure and its interactions with the hydrophobic core at H4 [41]. Consequently, this elucidates why variant H3.3 alone has minimal effect on nucleosome stability, as it is improbable to modify the histone-DNA interactions near SHL-2/2.

 doi:10.20944/preprints202403.1829.v1

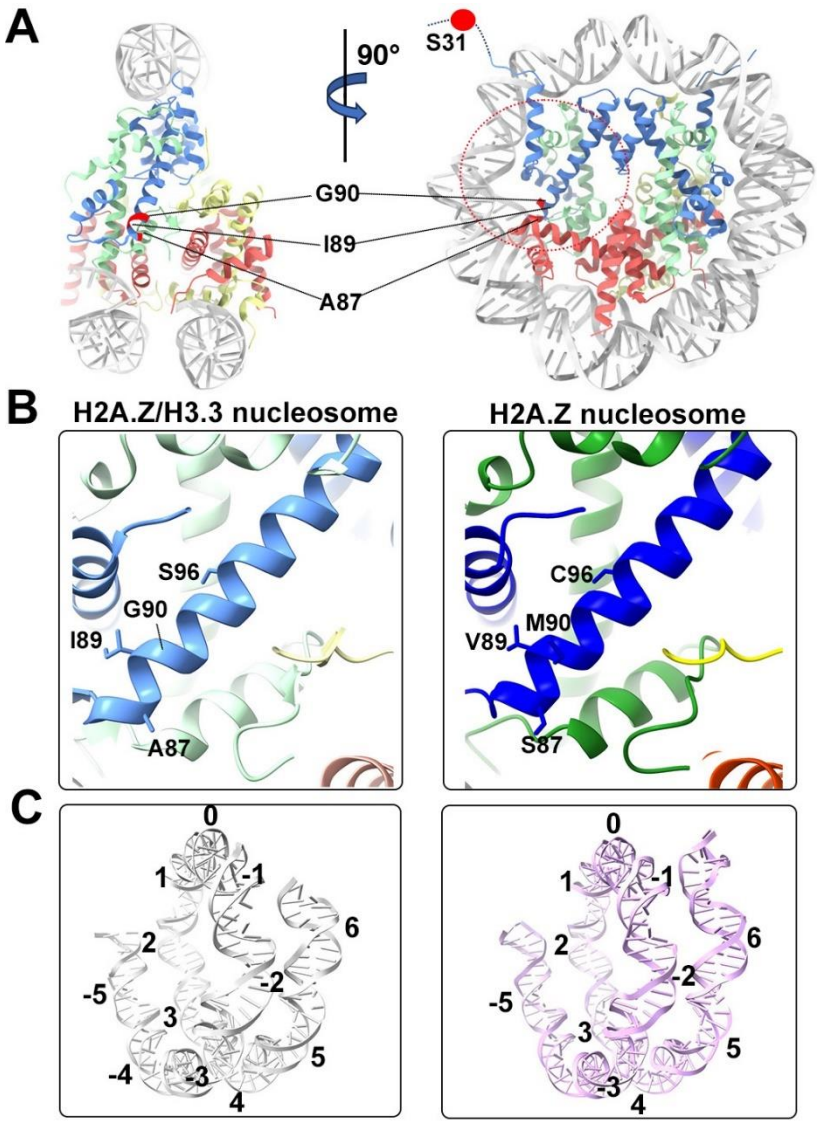

Figure 4. Structural comparison of H2A.Z and double-variant nucleosomes. (**A**) The five H3.3-specific residues are highlighted and labeled in the current model. (**B**) Close-up view of the H3.3 *a*2 helix region (red dotted oval in (**A**)) in the H2A.Z-H3.3 nucleosome (left). The same region of histone H3.1 in the H2A.Z nucleosome is shown (right, PDB ID 71MX). The four H3.3-specific residues and their counterparts in H3.1 are labeled. (**C**) Comparison of the DNA of H2A.Z-H3.3 nucleosome (left) with the DNA of the H2A.Z nucleosome, showing slightly longer/more resloved DNA ends beyond SHL6 in the H2A.Z nucleosome. The superhelical locations are labeled.

3.3. INO80-Mediated Nucleosome Sliding on H2A.Z- H3.3 Double-Variant Nucleosomes

Next, we sought to investigate the impact of variant H3.3 on ATP-dependent chromatin remodeling, specifically focusing on its potential influence on nucleosome-remodeler interaction and remodeling efficiency. Notably, a recent proteomics study revealed an association of INO80 with H3.3, but not with H3.1 [42]. To further investigate the functional consequence of H3.3 on INO80 activity, we conducted in vitro nucleosome sliding assays using the recombinant yeast INO80 complex (also known as INO80-C). The INO80 complex, an evolutionary conserved chromatin remodeler, is known to participate in various DNA metabolic processes, including transcription, replication, and damage repairs [43]. Like other members of the chromatin remodeler superfamily, INO80 exhibits typical remodeling activities such as mobilizing nucleosomes locally and influencing nucleosome spacing in vivo [43,44]. These functions are attributed to the enzyme's capacity to reposition nucleosomes along DNA in an ATP-dependent manner [45]. Notably, H2A.Z-nucleosomes

 doi:10.20944/preprints202403.1829.v1

are recognized as better substrates for INO80 compared to canonical nucleosomes in the nucleosome sliding assay [46].

We used end-positioned nucleosomes (0N80) to assess the DNA translocation activity of INO80-C across various nucleosome substrates. Specifically, we compared the INO80-C-mediated nucleosome sliding on H3.3, H2A.Z, and H2A.Z-H3.3 double-variant nucleosomes with canonical nucleosomes serving as the control. Our findings reveal that both H2A.Z and H2A.Z-H3.3 nucleosomes equally enhance the DNA-translocation activity of the complex, evidenced by nearly 100% of end-positioned nucleosomes were shifted to center-position after 10 minutes (**Figure S3**). In contrast, INO80 only shifted half of the canonical and H3.3 nucleosome substrates from the end to the center position (**Figure S3**). Consistent results were obtained from two additional independent experiments. These results suggest that variant H3.3 does not alter nucleosome properties that influence INO80-dependent nucleosome sliding.

4. Discussion

In our current study, we utilized Cryo-EM and biochemical assays to characterize the H2A.Z-H3.3 double-variant nucleosome. Our findings demonstrate that variant H3.3 incorporation does not significantly alter entry/exit DNA dynamics in nucleosomes. However, when variant H3.3 coexists with H2A.Z in the same nucleosome, the nucleosome exhibits enhance terminal DNA mobility and accessibility as observed in the presence of H2A.Z alone. Our Cryo-EM analysis further supports this observation, revealing that the H2A.Z-H3.3 double-variant nucleosomes adopt a nearly identical conformation to H2A.Z nucleosomes.

The atomic model of double-variant nucleosome shows that four H3.3-specific residues in the α2 helix does not cause detectable changes in any secondary structural elements in the histone core. This is consistent with the observation that H3.3 alone has minimal effects on nucleosome stability. Interestingly, our MNase digestion assay reveals a small but significant difference between H2A.Z and double-variant nucleosomes, where DNA near SHL-5.5/5.5 is more protected in double-variant nucleosomes compared to H2A.Z nucleosomes. These results suggest that the concurrent presence of H3.3 on H2A.Z nucleosomes offers an additional mechanism to fine-tune nucleosome DNA accessibility and thus the chromatin environment.

Finally, we demonstrate that the sole presence of variant H3.3 does not affect ATP-dependent INO80-mediated nucleosome repositioning, while double-variant nucleosomes behave similarly to H2A.Z nucleosomes in stimulating the DNA-translocation activity of INO80. These findings suggest that H3.3-mediated nucleosome changes rely on its co-occupancy with H2A.Z in the same nucleosome. Future studies will focus on investigating how the H3.3 variant influences higher-order chromatin structures.

Supplementary Materials: The following supporting information can be downloaded at the website of this paper posted on Preprints.org.

Author Contributions: V. Sokolova., G.L., H.J. and V. Stevens. prepared the samples for the cryo-EM study. H.J. and G.L. performed the biochemical analysis and H.J. and V.Sokolova performed the quantification; H.J. performed image processing and model building under the supervision of D.T.; D.T. oversaw the project and V.Sokolova and D.T. wrote the manuscript with help from all authors.

Funding: Research reported in the current study was supported by the National Science Foundation under award number 1942049 and by the National Institute of General Medical Sciences of NIH under award number 1R35GM133611. A portion of this research was supported by NIH grant U24GM129547 and performed at the University of Virginia Molecular Microscopy Core. A portion of the research was also supported by NIH grant 1S10OD012272-01A1 and performed at the cryo-EM facility at the Stony Brook University.

Data Availability and Accession Numbers: The data that support the findings of this study are openly available in the Electron Microscopy Database (https://www.ebi.ac.uk/pdbe/emdb) and the Protein Data Bank (https://www.rcsb.org/). The EM map of H2A.Z-H3.3 double-variant nucleosome is deposited at the Electron Microscopy Database under accession code EMD-44148. The corresponding protein coordinate is deposited at the Protein Data Bank under accession code PDB ID 9B3P.

 doi:10.20944/preprints202403.1829.v1

Acknowledgments: We thank Kelly Dryden and Michael Purdy for their assistant in cryo-EM data collection at the UVa Molecular Microscopy Core. .

Conflicts of Interest: The authors declare no competing interests. .

References

1. H. Tagami, D. Ray-Gallet, G. Almouzni, Y. Nakatani, Histone H3.1 and H3.3 complexes mediate nucleosome assembly pathways dependent or independent of DNA synthesis. *Cell* **116**, 51-61 (2004).
2. D. Brush, J. B. Dodgson, O. R. Choi, P. W. Stevens, J. D. Engel, Replacement variant histone genes contain intervening sequences. *Mol Cell Biol* **5**, 1307-1317 (1985).
3. I. Maze, K. M. Noh, A. A. Soshnev, C. D. Allis, Every amino acid matters: essential contributions of histone variants to mammalian development and disease. *Nat Rev Genet* **15**, 259-271 (2014).
4. M. J. Clarkson, J. R. Wells, F. Gibson, R. Saint, D. J. Tremethick, Regions of variant histone His2AvD required for Drosophila development. *Nature* **399**, 694-697 (1999).
5. R. Faast *et al.*, Histone variant H2A.Z is required for early mammalian development. *Curr Biol* **11**, 1183-1187 (2001).
6. X. Liu, B. Li, GorovskyMa, Essential and nonessential histone H2A variants in Tetrahymena thermophila. *Mol Cell Biol* **16**, 4305-4311 (1996).
7. P. Ridgway, K. D. Brown, D. Rangasamy, U. Svensson, D. J. Tremethick, Unique residues on the H2A.Z containing nucleosome surface are important for Xenopus laevis development. *J Biol Chem* **279**, 43815-43820 (2004).
8. S. Hardy *et al.*, The euchromatic and heterochromatic landscapes are shaped by antagonizing effects of transcription on H2A.Z deposition. *PLoS Genet* **5**, e1000687 (2009).
9. R. M. Raisner *et al.*, Histone variant H2A.Z marks the 5' ends of both active and inactive genes in euchromatin. *Cell* **123**, 233-248 (2005).
10. T. A. Soboleva *et al.*, A unique H2A histone variant occupies the transcriptional start site of active genes. *Nat Struct Mol Biol* **19**, 25-30 (2011).
11. C. M. Weber, J. G. Henikoff, S. Henikoff, H2A.Z nucleosomes enriched over active genes are homotypic. *Nat Struct Mol Biol* **17**, 1500-1507 (2010).
12. H. Zhang, D. N. Roberts, B. R. Cairns, Genome-wide dynamics of Htz1, a histone H2A variant that poises repressed/basal promoters for activation through histone loss. *Cell* **123**, 219-231 (2005).
13. S. John *et al.*, Interaction of the glucocorticoid receptor with the chromatin landscape. *Mol Cell* **29**, 611-624 (2008).
14. E. L. Sutcliffe *et al.*, Dynamic histone variant exchange accompanies gene induction in T cells. *Mol Cell Biol* **29**, 1972-1986 (2009).
15. M. M. Wong, L. K. Cox, J. C. Chrivia, The chromatin remodeling protein, SRCAP, is critical for deposition of the histone variant H2A.Z at promoters. *J Biol Chem* **282**, 26132-26139 (2007).
16. I. K. Greaves, D. Rangasamy, P. Ridgway, D. J. Tremethick, H2A.Z contributes to the unique 3D structure of the centromere. *Proc Natl Acad Sci U S A* **104**, 525-530 (2007).
17. D. Rangasamy, L. Berven, P. Ridgway, D. J. Tremethick, Pericentric heterochromatin becomes enriched with H2A.Z during early mammalian development. *EMBO J* **22**, 1599-1607 (2003).
18. S. D. Farris *et al.*, Transcription-induced chromatin remodeling at the c-myc gene involves the local exchange of histone H2A.Z. *J Biol Chem* **280**, 25298-25303 (2005).
19. N. Gevry, H. M. Chan, L. Laflamme, D. M. Livingston, L. Gaudreau, p21 transcription is regulated by differential localization of histone H2A.Z. *Genes Dev* **21**, 1869-1881 (2007).
20. A. S. Kotekar, J. D. Weissman, A. Gegonne, H. Cohen, D. S. Singer, Histone modifications, but not nucleosomal positioning, correlate with major histocompatibility complex class I promoter activity in different tissues in vivo. *Mol Cell Biol* **28**, 7323-7336 (2008).
21. I. Latorre *et al.*, The DREAM complex promotes gene body H2A.Z for target repression. *Genes Dev* **29**, 495-500 (2015).
22. A. Lashgari, J. F. Millau, P. E. Jacques, L. Gaudreau, Global inhibition of transcription causes an increase in histone H2A.Z incorporation within gene bodies. *Nucleic Acids Res* **45**, 12715-12722 (2017).
23. T. S. Lewis, V. Sokolova, H. Jung, H. Ng, D. Tan, Structural basis of chromatin regulation by histone variant H2A.Z. *Nucleic Acids Res* **49**, 11379-11391 (2021).
24. M. Zhou *et al.*, Structural basis of nucleosome dynamics modulation by histone variants H2A.B and H2A.Z.2.2. *EMBO J* **40**, e105907 (2021).
25. A. D. Goldberg *et al.*, Distinct factors control histone variant H3.3 localization at specific genomic regions. *Cell* **140**, 678-691 (2010).
26. C. Jin *et al.*, H3.3/H2A.Z double variant-containing nucleosomes mark 'nucleosome-free regions' of active promoters and other regulatory regions. *Nat Genet* **41**, 941-945 (2009).

 doi:10.20944/preprints202403.1829.v1

27. B. E. Schwartz, K. Ahmad, Transcriptional activation triggers deposition and removal of the histone variant H3.3. *Genes Dev* **19**, 804-814 (2005).
28. C. Jin, G. Felsenfeld, Nucleosome stability mediated by histone variants H3.3 and H2A.Z. *Genes Dev* **21**, 1519-1529 (2007).
29. H. Tachiwana *et al.*, Structures of human nucleosomes containing major histone H3 variants. *Acta Crystallogr D Biol Crystallogr* **67**, 578-583 (2011).
30. P. Chen *et al.*, H3.3 actively marks enhancers and primes gene transcription via opening higher-ordered chromatin. *Genes Dev* **27**, 2109-2124 (2013).
31. A. Thakar *et al.*, H2A.Z and H3.3 histone variants affect nucleosome structure: biochemical and biophysical studies. *Biochemistry* **48**, 10852-10857 (2009).
32. V. Sokolova, S. Sarkar, D. Tan, Histone variants and chromatin structure, update of advances. *Comput Struct Biotechnol J* **21**, 299-311 (2023).
33. P. N. Dyer *et al.*, Reconstitution of nucleosome core particles from recombinant histones and DNA. *Methods Enzymol* **375**, 23-44 (2004).
34. S. Q. Zheng *et al.*, MotionCor2: anisotropic correction of beam-induced motion for improved cryo-electron microscopy. *Nat Methods* **14**, 331-332 (2017).
35. A. Rohou, N. Grigorieff, CTFFIND4: Fast and accurate defocus estimation from electron micrographs. *J Struct Biol* **192**, 216-221 (2015).
36. J. Zivanov *et al.*, New tools for automated high-resolution cryo-EM structure determination in RELION-3. *Elife* **7**, (2018).
37. E. C. Meng *et al.*, UCSF ChimeraX: Tools for structure building and analysis. *Protein Sci* **32**, e4792 (2023).
38. P. Emsley, K. Cowtan, Coot: model-building tools for molecular graphics. *Acta Crystallogr D Biol Crystallogr* **60**, 2126-2132 (2004).
39. P. D. Adams *et al.*, PHENIX: a comprehensive Python-based system for macromolecular structure solution. *Acta Crystallogr D Biol Crystallogr* **66**, 213-221 (2010).
40. T. Schalch, S. Duda, D. F. Sargent, T. J. Richmond, X-ray structure of a tetranucleosome and its implications for the chromatin fibre. *Nature* **436**, 138-141 (2005).
41. K. Luger, A. W. Mader, R. K. Richmond, D. F. Sargent, T. J. Richmond, Crystal structure of the nucleosome core particle at 2.8 A resolution. *Nature* **389**, 251-260 (1997).
42. R. Siddaway *et al.*, The in vivo Interaction Landscape of Histones H3.1 and H3.3. *Mol Cell Proteomics* **21**, 100411 (2022).
43. X. Shen, G. Mizuguchi, A. Hamiche, C. Wu, A chromatin remodelling complex involved in transcription and DNA processing. *Nature* **406**, 541-544 (2000).
44. M. Papamichos-Chronakis, C. L. Peterson, The Ino80 chromatin-remodeling enzyme regulates replisome function and stability. *Nat Struct Mol Biol* **15**, 338-345 (2008).
45. V. Sokolova *et al.*, DNA-translocation-independent role of INO80 remodeler in DNA damage repairs. *J Biol Chem* **299**, 105245 (2023).
46. O. Willhoft, R. Bythell-Douglas, E. A. McCormack, D. B. Wigley, Synergy and antagonism in regulation of recombinant human INO80 chromatin remodeling complex. *Nucleic Acids Res* **44**, 8179-8188 (2016).